3D INTERACTIVE CORONARY ARTERY SEGMENTATION USING RANDOM FORESTS AND MARKOV RANDOM FIELD OPTIMIZATION

*Jingjing Deng, Xianghua Xie**

Department of Computer Science
Swansea University, United Kingdom
http://csvision.swan.ac.uk

Rob Alcock[1], *Carl Roobottom*[2]

[1]Peninsular Radiology Academy,
[2]Plymouth University Schools of
Medicine & Dentistry
Plymouth Hospitals NHS Trust, United Kingdom

ABSTRACT

Coronary artery segmentation plays a vital important role in coronary disease diagnosis and treatment. In this paper, we present a machine learning based interactive coronary artery segmentation method for 3D computed tomography angiography images. We first apply vessel diffusion to reduce noise interference and enhance the tubular structures in the images. A few user strokes are required to specify region of interest and background. Various image features for detecting the coronary arteries are then extracted in a multi-scale fashion, and are fed into a random forests classifier, which assigns each voxel with probability values of being coronary artery and background. The final segmentation is carried through an MRF based optimization using primal dual algorithm. A connectivity component analysis is carried out as post processing to remove isolated, small regions to produce the segmented coronary arterial vessels. The proposed method requires limited user interference and achieves robust segmentation results.

Index Terms— Coronary artery, interactive segmentation, random forests, Markov random field, primal dual algorithm

1. INTRODUCTION

Accurate segmentation algorithm for extracting the vessel structure is often considered essential for patient-specific treatment of cardiovascular diseases. A number of vessel extraction methods for different modalities have been developed in recent years, e.g. [1, 2, 3]. Li and Yezzi [2] proposed a 4-D representation for 3-D vessel by combining both the spatial coordinates and the thickness of the vessel. With two user specified endpoints, the surface as well as the center line of the vessel are extracted using the generalized 4-D global minimal paths algorithm. Esneault *et al.* [4] proposed a 3-D geometrical moment-based detector to extract the center line of the vessel, as well as its diameter and orientation. Then a graph cut algorithm was applied to regularize the final segmentation with a local continuity constraint. In [5], shape prior of 3D tubular tree structure is used to formulate the regularization to refine the initial vessel segmentation or detection. Zhu and Chung [6] proposed the TMT (Tubularity Markov Tree) method to model and detects vessel structure, with a graph cut algorithm applied to solve the energy minimization problem in order to obtain the final segmentation. Deformable models, particularly those that are capable of capturing complex geometries such as [7], may be applied to vessel segmentation. Efficient model representation and numerical methods are desirable and semi-implicit schemes have been shown effective in segmenting complex objects, e.g. [8, 9].

The segmentation of coronary artery is not a trivial problem. First, the coronary artery are attached to the myocardium and surrounded by other tissues. Second, compared to the aorta, the size of the coronary artery is much smaller, which makes it difficult to segment and maintain its vessel connectivity. Last but not least, there are several other blood vessel nearby, such as pulmonary blood vessel in the lung, which has very similar appearance and geometry. This makes an automated, global detection or classification a difficult task. In this paper, we present an interactive coronary artery 3D segmentation method for computed tomography angiography (CTA) volumetric image. An initial vessel classification is given by a random forest classifier which is trained on a few user strokes: the foreground stroke labels the coronary artery and the background stroke indicates the other tissues. Based on the label population in the leaf nodes of the randomized decision trees, we formulate the final segmentation as an MRF based optimization with local consistency constraints. The primal dual algorithm with graph cut is used to solve the energy minimization problem.

The rest of the paper is organized as following. Sec. 2 presents our proposed approach including vessel enhancement, feature extraction, RF classification and MRF optimization. The results are presented in Sec. 3, and Sec. 4 concludes the paper.

*Correspondence: x.xie@swansea.ac.uk

2. METHODOLOGY

2.1. Vessel Enhancing Diffusion

It is desirable to enhance the brightness of coronary vessel and the sharpness of vessel edges in 3D before carrying out segmentation, particularly for this type of thin tubular structures. Frangi et al. [10] proposed a vesselness function by analyzing the eigenvalues of the second order information (Hessian) in a local neighborhood at multiple scales. The eigenvalues decomposed from the Hessian matrix were used to locally differentiate the tubular-like structure from other structures, including blob-like structure, plate-like structure and background. Manniesing *et al.* [11] extended it to a continuous, n-th order differentiable function for measuring the vesselness. Based on the proposed vesselness function, the diffusion tensor was constructed to enhance the image at vessel region along minimal local curvature direction, while smoothing the image isotropically at non-vessel region. In this work, we follow this approach to enhance the coronary vessel structures in the CTA images. Later, the measurements derived from this vesselness analysis are also used as part of the coronary features.

2.2. Multi-Scale Coronary Feature Extraction

The features we use to highlight coronary vessels can be categorized as texture or appearance based and shape based. The texture features are derived as intensity and image gradient magnitude distribution in a local neighborhood across multiple scales. These appearance features are useful in differentiating myocardium, bone, and adventitia. Since they are extracted from multiple scales, the difference between other vascular structures and coronary vessels can be highlighted. For example, although aorta exhibits similar brightness to coronary, it has different intensity distribution across scales because aorta is a much larger vessel. Pulmonary vessels has similar geometry to coronary arteries but their neighborhood appearances are different.

The second set of features are designed to highlight the narrow, tubular-like structure of coronary vessels. We derive multiscale local geometrical features, following those that have been used in vessel enhancement. At scale $\mathcal{S}$, the Hessian matrix $\mathcal{H}$ at each voxel $\mathcal{P}$ is computed by convolving the volumetric image with derivatives of Gaussian. The eigenvalues λ of Hessian matrix are then computed. In the case of 3D, we define the ordering eigenvalues as $\mathcal{H}$ as $\lambda_1, \lambda_2, \lambda_3$, where $|\lambda_1| \leq |\lambda_2| \leq |\lambda_3|$. At scale s, the eigenvalues of Hessian indicate the strengths of intensity variation between the inside and outside of the region $(-s, s)$ along the direction of the corresponding eigenvectors. The coronary vessels are assumed at the region in which $|\lambda_1| \approx 0$, $|\lambda_1| \ll |\lambda_2|$, $\lambda_2 \approx \lambda_3$, while the eigenvector corresponding to the eigenvalue λ_1 indicates the vessel direction. We adopt the Manniesing's vesselness function $\mathcal{V}$, which is defined as follows:

$$\mathcal{V} \triangleq \begin{cases} 0 & \lambda_2 \geq 0 \; or \; \lambda_3 \geq 0 \\ (1 - e^{\frac{-A^2}{2\alpha^2}}) \cdot e^{\frac{-B^2}{2\beta^2}} \cdot (1 - e^{\frac{-S^2}{2\gamma^2}}) \cdot e^{\frac{2c^2}{|\lambda_2|\lambda_3^2}} & otherwise \end{cases}$$

where

$$A = \frac{|\lambda_2|}{|\lambda_3|}, \;\; B = \frac{|\lambda_1}{\sqrt{|\lambda_2 \lambda_3|}}, \;\; S = \sqrt{\lambda_1^2 + \lambda_2^2 + \lambda_3^2} \tag{1}$$

The parameters α, β, γ are the weighting variables controlling the contributions of the measurements to the response of vesselness function. The vesselness measurement are computed at multiple scales and the maximum response $\mathcal{V}$ over the scale-spaces is selected.

2.3. Voxel Classification using Random Forests

Random forests [12] is a supervised machine learning method which aims to overcome the problems caused by poor generalization ability of single decision tree. In our work, classifying each voxel into coronary and non-coronary is required so that the confidence value of the classification at each voxel is used to construct the cost function for the MRF based optimization.

Random forests grows a number of decision trees independently using subsets of training data by randomly sampling with replacement from the complete training set. For each single decision tree, it grows recursively by finding the best splitting function for each non-leaf node using the entropy or Gini index to evaluate the information loss, until the stopping criteria are satisfied. The non-leaf nodes consist of the splitting functions, each testing sample could follow the tests and reach the leaf node in the end. The leaf nodes, at the bottom layer of the tree, store the training samples which fell in in the training stage, and it votes the class with largest proposition for the prediction. The random forests combines the prediction of each single decision tree, the most voted class given by the forests is considered as the final classification for the test sample. From the implementation point of view, the random forests is supremely adequate for paralleling. By taking advantage of GPU computing technique, classifying each pixel of a 500×300 2D image can be achieved in 140ms. [13]

In our work, 3D MPR (Multi-Planar Reconstruction) and curved MPR are used to produce the longitudinal view of the coronary artery, in which a few strokes are placed to indicate the region of interest at the foreground. Also, the non-coronary artery tissues, such as: aorta, ventricle, heart muscle, pulmonary blood vessels and so on, are obtained through additional user strokes as background, negative samples. We sample the voxels following the strokes with equal spacing, and the features of those voxels as described in Sec. 2.2 are collected as training set. Then the whole volume is tested, the classification result may be considered as an initial segmentation. However, the proposition of voting by these randomized decision trees for each voxel can be considered as segmentation cue. In the next section, we show how to use these proposition values to carry out segmentation that can be more coherent than RF classification.

2.4. Segmentation using MRF Optimization with Primal Dual Algorithm

MRF has been widely applied in different computer vision applications to address the regularization problems. Especially, the grid-like, pairwise MRF model in image segmentation area has shown to be an effective approach, e.g. [14]. In general, the MRF energy is formulated over the graph $G(\mathcal{P}, \mathcal{E})$ as follows:

$$E(p) = \sum_{i \in \mathcal{P}} U(p_i) + \sum_{<i,j> \in \mathcal{E}} O(p_i, p_j) \tag{2}$$

where $\mathcal{P}$ and $\mathcal{E}$ represent the node set and the two-tuples set of undirected edge of G respectively. $U(.)$ is the unary potentials defined on the node $\mathcal{P}$, and $O(.)$ is the pairwise potentials defined on the edge $\mathcal{E}$. The first term of Eq. 2 is considered as point-wise data term which provides the segmentation cue, the second term is considered as pair-wise smoothness term which constrains the consistency between neighbour nodes. For example, the Potts pairwise potentials is defined on the distance of two linked nodes x_i, x_j, as follows:

$$O(p_i, p_j) = w_{ij} \cdot (1 - \delta(p_i - p_j)) \tag{3}$$

where $w_{ij} \geq 0$ is the weighting coefficient of smoothing penalty for the edge $< i, j >$, and the Kronecker delta δ is defined as:

$$\delta(p) = \begin{cases} 1 & x = 0 \\ 0 & x = 1 \end{cases} \tag{4}$$

Here, the segmentation is to assign each voxel/vertex with a label l_p ($l_p \in \mathcal{L}$; $l_p = 1$ when p is coronary artery; $l_p = 0$ when p is not). In Sec. 2.3, the binary classification result of each vertex is given by the classifier as well as the voting proposition k_{l_p} which could be considered as the likelihood or confidence of being categorized to the class. So, the regularization can be formulated as solving the discrete MRF optimization problem by minimizing the following MRF energy function:

$$min \left(\sum_{p \in \mathcal{P}} U(p) + \sum_{<p,q> \in \mathcal{E}} O(p, q) \right) \tag{5}$$

In binary classification case, we have $k_{l_p=0} = 1 - k_{l_p=1}$, so the point-wise potentials is defined as:

$$U(p) = \begin{cases} T(1 - k_{l_p=1}) & if \quad l_p = 1 \\ T(1 - k_{l_p=0}) & if \quad l_p = 0 \end{cases} \tag{6}$$

which implies, for example, the cost of assigning the class label 0 to the vertex p is equal to $T(1 - k_{l_p=1}) = T(k_{l_p=0})$, the non-linear transformation of the confidence of assigning it with label 1. One of disadvantage of graph-cut based method is the shrink bias which results in smaller contour, and becomes even worse in the corner region. The goal of the non-linear transformation function T is to enlarge the difference between $k_{l_p=0}$ and $k_{l_p=1}$ when their values are getting similar, which is very common for the vertexes around the vessel surfaces. By applying the non-linear transformation, to a large extent, the shrink bias caused by the pair-wise term will be reduced. We propose the following non-linear transformation function T:

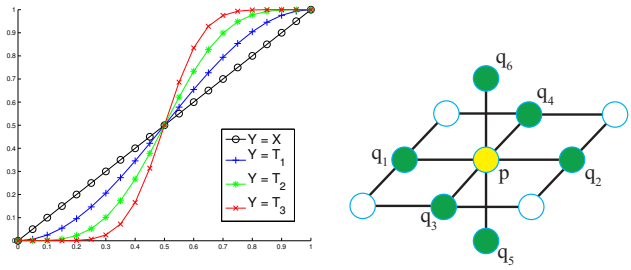

(a) (b)

Fig. 1. (a) Non-linear transformation function $T_{\eta=1,2,3}$ compared to the linear function $Y = X$. (b) MRF with 6 neighbourhood system, $< p, q_{1,\cdots,6} >$.

$$T_\eta(k) = \overbrace{t \circ t \circ \cdots \circ t}^{\eta} \tag{7}$$

$$t(k) = \frac{1}{2} + \frac{1}{2} \sin(\pi k - \frac{\pi}{2}) \tag{8}$$

where $\circ$ is the function composition operator (see Fig. 1). It can be proved that $T_\eta(1-k) = 1 - T_\eta(k)$ when $k \in [0, 1]$. In addition, we use grid-like MRF with 6-neighbourhoods system in our experiment, and choose the Potts model as pair-wise potentials (see Eq. 3, 4).

A number of approaches have been proposed in the literature to solve the energy minimization problem of discrete pair-wise MRF, such as graph cuts based methods [15, 16], and belief propagation algorithm [17]. Especially, the dual-decomposition approach with linear programming method attracts a great attention in the last decade [18]. Chekuri et al. [19] have proved that the solution of metric labeling problem given by the form of minimizing the MRF energy (Eq. 5) can be approximated using the following integer programming formulation:

$$min \left(\sum_{p \in \mathcal{P}, a \in \mathcal{L}} c_p(a) x_p(a) + \sum_{<p,q> \in \mathcal{E}} w_{pq} \sum_{a,b \in \mathcal{L}} d(a, b) x_{pg}(a, b) \right) \tag{9}$$

which subjects to the following constrains:

$$\sum_{a \in \mathcal{L}} x_p(a) = 1 \qquad \forall p \in \mathcal{P} \tag{10}$$

$$\sum_{a \in \mathcal{L}} x_{pg}(a, b) = x_q(b) \quad \forall b \in \mathcal{L}, < p, q > \in \mathcal{E} \tag{11}$$

$$\sum_{b \in \mathcal{L}} x_{pg}(a, b) = x_p(a) \quad \forall a \in \mathcal{L}, < p, q > \in \mathcal{E} \tag{12}$$

where $x_p(.) = 0, 1$, and $x_{pq}(., .) = 0, 1$. The constrain Eq. 10 ensures for each vertex p, a label is assigned to, and the constrains Eq. 11 and 12 ensure the consistency of the label between the neighbors. Komodakis *et al.* gave the solution of above optimization problem Eq. 9 via dual decomposition, and proposed a family of PD (Primal-Dual) algorithms.

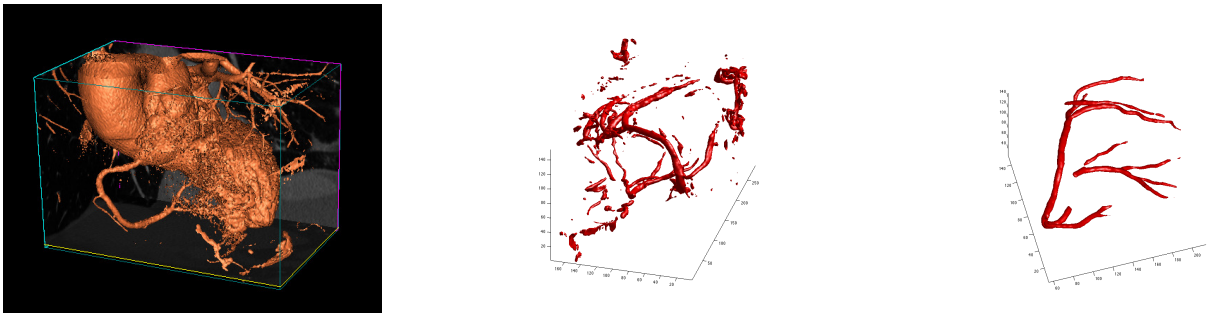

(a) (b) (c)

Fig. 2. (a) iso-surface rendering of the CTA image; (b) RF based voxel classification result; (c): result of the proposed method.

In this work, the PD1 algorithm [20, 21] is adopted, which solves the decomposed sub-problems via Graph-cut in each iteration.

3. EXPERIMENTAL RESULTS

The method is evaluated on the clinical CTA volumes. The volumes have different number of slices with 0.65mm inter-slice spacing, each slice has 512×512 pixels with 0.38mm intra-slice spacing. At first, we cropped out the region of interest which contains the whole heart and a part of region in the lung, then followed by 10-iteration vessel enhancing diffusion filtering. The features for every vertex in the sub-volume are computed in multi-scale spaces with $\sigma \in \{0, 1, 2, 3, 4\}$, which results in a 85-components feature vector. A random forests classifier with 200 decision trees is interactively trained on the training set which provided by sampling the vertexs from the user's foreground and background strokes. The sub-volume is segmented by optimizing the classification result given by the random forests using grid-like Markov random field model with 6 neighbours system and PD1 algorithm. Given the binary volume, the segmented result is visualized as iso-surface using marching cube algorithm. Once the user adds more strokes, we repeat the classifier training, sub-volume classification, label optimization and result rendering processes, until no more user's stroke is detected, and the final segmentation is achieved. A connected component analysis was also carried out to remove isolated, small regions.

Fig. 2 provides an example of the segmentation process and result. In (a), we show the iso-surface rendering of the vascular structures, including the ventricles. It is clear from this that coronary vessels are only a small proportion of those structures. To isolate them and to obtain a coherent structure with good connectivity is not a trivial task. Fig. 2(b) shows the classification result from RF classifier. Most of the non-coronary structures are removed, but there are still plenty of isolated thin, tubular structures. The final result of the proposed method is shown in (c), where the coronary structures are well segmented. Two further examples are provided in Fig. 3. The examples provided here are typical results we achieve using the proposed method. The user interactions are minimal, i.e. only a few strokes on the foreground and background.

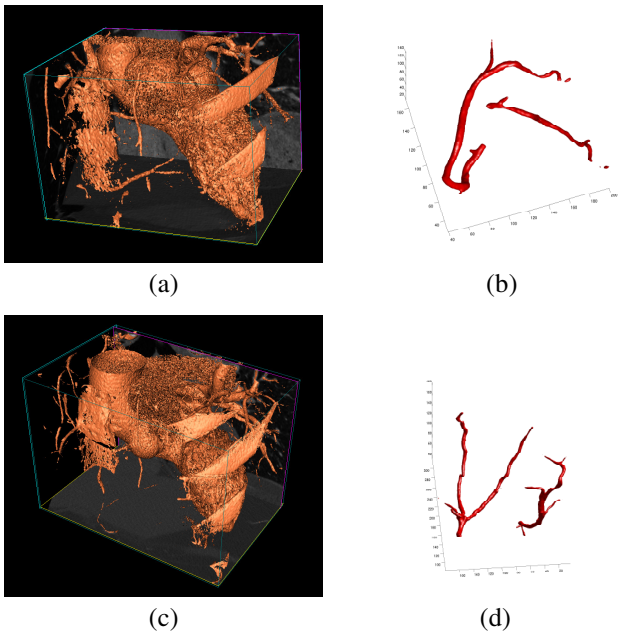

(a) (b) (c) (d)

Fig. 3. (a) (c) iso-surfaces rendering of the CTA images; (b) (d) results of the proposed method.

4. CONCLUSIONS

A 3D interactive segmentation method for coronary artery has been presented in this paper. The vessel enhancing diffusion filter is adopted to pre-process the volumetric image. Random forest classifier is trained on the feature which designed for discriminating the coronary artery from other tissues. The segmentation is achieved by regularizing the classification result with the constrain ensuring the local label consistency. Promising segmentation results are achieved with just a few user strokes.

5. REFERENCES

[1] Cemil Kirbas and Francis Quek, "A review of vessel extraction techniques and algorithms," *ACM Computing Survey*, vol. 36, no. 2, pp. 81–121, 2004.

[2] Hua Li and Anthony Yezzi, "Vessels as 4-d curves: Global minimal 4-d paths to extract 3-d tubular surfaces and centerlines," *IEEE Transactions on Medical Imaging*, vol. 26, pp. 1213–1223, 2007.

[3] David Lesage, Elsa D. Angelini, Isabelle Bloch, and Gareth Funka-Lea, "A review of 3d vessel lumen segmentation techniques: Models, features and extraction schemes," *Medical Image Analysis*, vol. 13, no. 6, pp. 819–845, 2009.

[4] Simon Esneault, Cyril Lafon, and J-L Dillenseger, "Liver vessels segmentation using a hybrid geometrical moments/graph cuts method," *IEEE Transactions on Biomedical Engineering*, vol. 57, no. 2, pp. 276–283, 2010.

[5] Christian Bauer, Thomas Pock, Erich Sorantin, Horst Bischof, and Reinhard Beichel, "Segmentation of interwoven 3d tubular tree structures utilizing shape priors and graph cuts," *Medical Image Analysis*, vol. 14, no. 2, pp. 172–184, 2010.

[6] Ning Zhu and Albert C.S. Chung, "Graph-based optimization with tubularity markov tree for 3d vessel segmentation," in *IEEE Conference on Computer Vision and Pattern Recognition*, June 2013, pp. 2219–2226.

[7] Xianghua Xie and Majid Mirmehdi, "Magnetostatic field for the active contour model: A study in convergence.," in *Proceedings of the British Machine Vision Conference*, 2006, pp. 127–136.

[8] Xianghua Xie and Majid Mirmehdi, "Implicit active model using radial basis function interpolated level sets.," in *Proceedings of the British Machine Vision Conference*, 2007, pp. 1–10.

[9] Xianghua Xie and Majid Mirmehdi, "Radial basis function based level set interpolation and evolution for deformable modelling," *Image and Vision Computing*, vol. 29, no. 2, pp. 167–177, 2011.

[10] Alejandro F Frangi, Wiro J Niessen, Koen L Vincken, and Max A Viergever, "Multiscale vessel enhancement filtering," in *Proceedings of Medical Image Computing and Computer-Assisted Interventation*, 1998, vol. 1496, pp. 130–137.

[11] Rashindra Manniesing, Max A. Viergever, and Wiro J. Niessen, "Vessel enhancing diffusion: A scale space representation of vessel structures," *Medical Image Analysis*, vol. 10, no. 6, pp. 815–825, 2006.

[12] Leo Breiman, "Random forests," *Machine learning*, vol. 45, no. 1, pp. 5–32, 2001.

[13] Jakob Santner, Markus Unger, Thomas Pock, Christian Leistner, Amir Saffari, and Horst Bischof, "Interactive texture segmentation using random forests and total variation," in *Proceedings of the British Machine Vision Conference*, 2009, pp. 66.1–66.12.

[14] Chaohui Wang, Nikos Komodakis, and Nikos Paragios, "Markov random field modeling, inference & learning in computer vision & image understanding: A survey," *Computer Vision and Image Understanding*, vol. 117, no. 11, pp. 1610–1627, 2013.

[15] Pushmeet Kohli, Jonathan Rihan, Matthieu Bray, and Philip HS Torr, "Simultaneous segmentation and pose estimation of humans using dynamic graph cuts," *International Journal of Computer Vision*, vol. 79, no. 3, pp. 285–298, 2008.

[16] Carsten Rother, Vladimir Kolmogorov, and Andrew Blake, "Grabcut: Interactive foreground extraction using iterated graph cuts," *ACM Transactions on Graphics*, vol. 23, no. 3, pp. 309–314, Aug. 2004.

[17] Jian Sun, Nan-Ning Zheng, and Heung-Yeung Shum, "Stereo matching using belief propagation," *IEEE Transactions on Pattern Analysis and Machine Intelligence*, vol. 25, no. 7, pp. 787–800, 2003.

[18] Nikos Komodakis, Georgios Tziritas, and Nikos Paragios, "Performance vs computational efficiency for optimizing single and dynamic mrfs: Setting the state of the art with primal-dual strategies," *Computer Vision and Image Understanding*, vol. 112, no. 1, pp. 14–29, 2008.

[19] Chandra Chekuri, Sanjeev Khanna, Joseph Seffi Naor, and Leonid Zosin, "Approximation algorithms for the metric labeling problem via a new linear programming formulation," in *Proceedings of ACM-SIAM Symposium on Discrete Algorithms*, 2001, pp. 109–118.

[20] Nikos Komodakis and Georgios Tziritas, "Approximate labeling via graph cuts based on linear programming," *IEEE Transactions on Pattern Analysis and Machine Intelligence*, vol. 29, no. 8, pp. 1436–1453, 2007.

[21] Nikos Komodakis, Nikos Paragios, and Georgios Tziritas, "Mrf energy minimization and beyond via dual decomposition," *IEEE Transactions on Pattern Analysis and Machine Intelligence*, vol. 33, no. 3, pp. 531–552, 2011.